Journal of Applied Pharmaceutical Science Vol. 13(02), pp 196-210, February, 2023
Available online at http://www.japsonline.com
DOI: 10.7324/JAPS.2023.141134
ISSN 2231-3354

Synthesis, spectroscopic characterization, thermal studies, and molecular docking of novel Cr(III), Fe(III), and Co(II) complexes based on Schiff base: *In vitro* antibacterial and antitumor activities

Samar A. Aly[1], Ayman Eldourghamy[1], Bahagat A. El-Fiky[1], Assmaa A. Megahed[1], Wael A. El-Sayed[2], Ehab M. Abdalla[3] Hussein H. Elganzory[2*]

[1]Department of Environmental Biotechnology, Genetic Engineering and Biotechnology Research Institute, University of Sadat City, Sadat City, Egypt.
[2]Department of Chemistry, College of Science, Qassim University, Buraidah, Saudi Arabia.
[3]Chemistry Department, Faculty of Science, New Valley University, Alkharga, Egypt.

ARTICLE INFO

Received on: 09/07/2022
Accepted on: 29/11/2022
Available Online: 05/02/2023

Key words:
Complexes, thermal studies, antibacterial activity, antitumor activity, and molecular docking.

ABSTRACT

New chelates complexes of general formulae $[Cr(H_2L)_2Cl_3.EtOH]$, $[Fe(H_2L)(OH)SO_4(H_2O).2H_2O]$, $[Fe(HL)_2(OH)].H_2O$, and $[Co(H_2L)(HL)_2.1/2\ EtOH]$ were prepared and identified by spectral techniques and thermogravimetric analysis Derivative thermo gravimetric analysis. The results confirmed that the ligand behaved as neutral tetradentate, bidentate, or monobasic tridentate. Coordination has occurred via carbonyl oxygen (C=O) and N(2)H or (C-S) groups in complex (3). Moreover, complex (3) was more stable than the analogs (1–3). The prepared mononuclear complexes exhibited an octahedral conformation. The ligand and Cr(III), Fe(III), and Co(II) complexes were investigated for their inhibitory action on the growth of *Streptococcus pyogenes* and *Escherichia coli* as Gram-positive and negative bacteria, respectively. The results indicated the effective behavior of Cr(III), Fe(III), and Co(II) complexes as being antibacterial compared to the ligand. The *in vitro* antitumor activity also displayed the potent action of compounds. In addition, it was revealed that the majority of complexes were more effective than their free ligand. Furthermore, molecular docking implementation demonstrated the intriguing possible interactions of the ligands and complexes with amino acid active sites of the ribosyltransferase moiety (PDB ID).

INTRODUCTION

Schiff-based ligands of thiosemicarbazones have gained significance over the decades as potential drug candidates (Nehar *et al*., 2020). Thiosemicarbazones are a group of compounds with numerous pharmacological applications, such as anti-inflammatory (Palaska *et al*., 2002), antibacterial (Plech *et al*., 2011), antifungal, antituberculosis (Küçükgüzel *et al*., 2006), antiviral (Pandeya *et al*., 1999), and antitumoral (de Oliveira *et al*., 2015) activities. The antitumoral activity of these compounds is due to their ability to restrain ribonucleotide reductase, which is an enzyme necessary for DNA synthesis (Sartorelli *et al*., 1970). Moreover, they have been proven to be good antiprotozoal, antioxidant, antimicrobial, and anticancer agents and have shown catalytic activities when coordinated with metals (Manikandan *et al*., 2015; Subarkhan and Ramesh, 2015). Several applications of these ligands have also been reported in the field of analytical chemistry (Garg and Jain, 1988; Pavon *et al*., 1975).

Furthermore, the role of transition metals as micronutrients as well as cofactors of various metalloenzymes in living systems reinforces the rationale beyond the preparation and quantification of new transition metal-based thiosemicarbazones complexes for their antitumor effects (Prajapati and Patel, 2019). When tested *in vivo*, the future use of alternative thiosemicarbazones as efficient anticancer drugs would rely on structural alterations that would

*Corresponding Author
Hussein H. Elganzory, Department of Chemistry, College of Science, Qassim University, Buraidah, Saudi Arabia.
E-mail: hhsien @ qu.edu.sa

confer improved potency against a variety of tumors/cancers, as well as lower toxicity and better solubility. Chromium (III) complexes showed certain biological activity, especially in regulating carbohydrates and lipid metabolism (Pechova and Pavlata, 2007). As an essential micronutrient, a low diet of chromium will exhibit several adverse effects, such as glucose intolerance, growth disorders, and diminished longevity (Jumina and Harizal, 2019). Iron is fundamental for normal cellular function. It is involved in a wide assortment of cellular processes, including DNA synthesis (Fuss *et al*., 2015; White and Dillingham, 2012; Zhang, 2014), cellular respiration, and macromolecule biosynthesis. Moreover, it is required for cell proliferation and growth, and changes in intracellular iron availability can have a significant impact on cell division, cell cycle regulation, and cellular metabolism (Arnold *et al*., 2016; Grodick *et al*., 2015; Paul and Lill, 2015). Neoplastic cells have higher iron requirements than normal, nonmalignant cells, which is somewhat unsurprising. Iron chelation has been investigated as a potential therapeutic intervention in many malignancies. Iron homeostasis has been studied in nonmalignant and malignant cells, the widespread effects of iron depletion on the cell, various iron chelators in cancer treatment, and the tumor types that have been most commonly studied in the context of iron chelation (Kalinowski and Richardson, 2005; Lieu *et al*., 2001; Merlot *et al*., 2013). Thiosemicarbazones are synthetic tridentate metal chelators that bind iron while also chelating other metals, including zinc and copper (Murphy *et al*., 2017; Tang *et al*., 2017). Because of their tridentate structure, thiosemicarbazones allow iron to participate in redox reactions (Basha *et al*., 2014). Additionally, the complexes derived from Schiff bases and Co(II) were reported to exhibit bactericidal, fungicidal, antitubercular, and antiviral activities (Lv *et al*., 2006).

This work aims to study the preparation and spectroscopic characterization of chromium, cobalt, and iron complexes of the ligand (4-(4-chlorophenyl)-1-(2-(phenylamino)acetyl) thiosemicarbazone)(H_2L) and to investigate the antibacterial and antitumor activities of newly synthesized compounds.

EXPERIMENT

Materials

All involved reactions were performed in atmospheric conditions. The utilized substrates and reagents are hydrazide, 4-chlorophenyl isothiocyanate, $CrCl_3.6H_2O$, $FeCl_3.6H_2O$, and $CoBr_2.6H_2O$, which were of AnalaR grade and were purchased from Sigma-Aldrich Chemie (Germany) and Fluka. Organic solvents were available at reagent grade without prior purification to prepare the ligand and complexes.

Preparation of (4-(4-chlorophenyl)-1-(2-(phenylamino)acetyl) thiosemicarbazone)

The substituted thiosemicarbazone (H_2L) was obtained by refluxing the hydrazide (0.01 mol) and the 4-chlorophenyl isothiocyanate (0.01 mol) in ethanol (10 ml) for 6 hours. Cooling the mixture gave the precipitated product, which was filtered, followed by washing with ethanol and diethyl ether, and then dried using vacuum (P_4O_{10}).

Preparation of metal complexes

An absolute ethanol solution (20 ml) containing 0.001 moles of metal salt (where M = Cr(III), Fe(III), and Co(II)) was added to a solution (30 ml) containing 0.001 moles of the (4-(4-chlorophenyl)-1-(2-(phenylamino)acetyl) thiosemicarbazone) (H_2L) and afforded mixture was stirred at 60°C for 4–7 hours; if any solid formed, the solution was directly filtered, or the solution was kept at 35°C to evaporate half of the solvent amount leading to crystallization followed by filtration and dryness.

Physical and spectral techniques

Various spectroscopic techniques were utilized to characterize the ligand (H_2L) and its derived complexes. Elemental analyses (C, H, and N) were investigated at the Microanalytical Unit of Cairo University, Egypt. The metal content was hydrolyzed with nitric acid and then estimated using EDTA following the standard methods. ^{1}H-NMR spectra in deuterated dimethyl sulfoxide d_6- Dimethylsulfoxide (DMSO) were recorded using a 300 MHz Varian nuclear magnetic resonance (NMR) spectrometer. The chemical shift was measured relative to the solvent peak. The Fourier transform infrared spectrography (FTIR) of ligands and complexes was completed at the Microanalytical Unit, Cairo University, Egypt, in the wavelength range (4000–400 cm^{-1}) using KBr discs and a Nenexeus-Nicolidite-640- MSAFT-IR FTIR infrared spectrophotometer. The electronic spectra (ultraviolet/visible) were recorded using a Perkin Elmer Lambda 330 spectrophotometer. The electronic spectra of the dimethylformamide (DMF) solution of each of the thiosemicarbazide ligand and metal complexes were recorded in 1 cm quartz cells. The molar conductivity measurements were determined in N, N′- DMF solution at (10^{-3}M) using a Tacussel conductometer type CD6N. Magnetic susceptibilities of the complexes were investigated by modifying the Gouy technique at r.t. utilizing Magnetic Susceptibility Johnson–Matthey Balance. The efficient moments were determined by applying the following relation: $\mu_{eff} = 2.828(\chi_m T)^{½}$ B.M, where μ_{eff} stands for magnetic susceptibility effective and χ_m is molar magnetic susceptibility.

Biological test

Bacterial strains and media

The *in vitro* antibacterial activity was studied at the Microbial Biotechnology Department, Genetic Engineering and Biotechnology Research Institute, University of Sadat City, Egypt, following the Broth Dilution Method. In the study, highly pathogenic *Streptococcus pyogenes* were isolated from human sources obtained from the soil of the Menoufia governorate and tested. Nutrient broth medium was prepared by using Brain heart infusion (BHI) broth medium (MP Bio) incorporated brain extract, heart extract, and peptones (27.5 g), D(+)-glucose (2 g), in addition to 5 g NaCl and 2.5 g of Na2HPO4 per l. The pH was set to 7.4 by adding diluted NaOH. The bacterial strains were grown utilizing the medium, and SK activity was monitored during the growth curve of the microbes. NB medium comprises 1 g D(+)-glucose, 15 g peptone, 6 g sodium chloride, and 3 g yeast extract per liter. The pH was regulated to be 7.4 using NaOH (Akhurst, 1982). The physiological saline solution incorporated NaCl 0.9 g/liter.

The antibacterial activity was investigated following a modified assay (Aly and El-Boraey, 2019) to study the inhibitory action of the resulting complexes and their hydrazide precursor against *S. pyogenes* (a type of Gram-positive organism) and *Escherichia coli* (Gram-negative species). The growing of *S. pyogenes* and *E. coli* cells was performed using BHI and Nutrient broth (NB) medium, respectively. With two concentrations of

DMSO, the investigated compounds were dissolved (1, 5, and 7µg/ml) n DMSO; then activation of bacterial strains on the proper broth media via shaking was carried out. A culture of bacteria was incubated at 37°C for 24 hours, and one of them was utilized as inoculation in the broth media, and the cultures of *S. pyogenes* and *E. coli* were inoculated to grow aerobically on BHI broth medium and NB medium. A spectrophotometer was used for calculating growth turbidity at 650 nm. After bacterial culture was grown on the media that included the tested derivatives and the control group, measurements were taken after 24 and 48 hours of incubation.

Antitumor activity

The antitumor activity of the synthesized complexes was investigated using a breast cancer cell line (MCF7, ATCC HTB-22). The cell line was maintained and propagated in Modified Eagle's Medium supplemented with 10% inactivated fetal calf serum, 2.4 sodium bicarbonate, 1 × 10^6 Penicillin units, 1 g Streptomycin, and 1 ml Garamycin 80, respectively (all chemicals and reagents are purely purchased from Sigma-Aldrich). The cell line was incubated in 5% CO_2 at 37°C to reach confluence; then cells were harvested using 1:250 trypsin enzyme. The viability of cells was examined with a 0.5% trypan blue stain. Then, cells were seeded in 8 × 12 microtiter plates at concentrations that can reach confluency 24 hours after withdrawal of the seeding growth medium, and different doses of metal complexes were titrated to investigate acute dose, lethal dose fifty (LD50), and therapeutic doses applied to a microtiter plate in another experiment to investigate the antitumor activity of metal complexes.

Superoxide dismutase (SOD)

SOD (Veiga *et al*., 2021) was performed according to the manufacturer's instructions. In brief diluted standard, the blank and samples were added to the appropriate well of plate precoated with an antibody specific to SOD, followed by incubation of plate for 2 hours at 37°C, washing, the addition of detection reagent working solution (100 ml), and incubation at the same temperature for 1 hour. Detection reagent B was added after washing the plate and 100 ml to each well, followed by incubation for 30 minutes at 37°C. The plate was washed, followed by the addition of substrate solution (990 ml) and incubation for 15 minutes at room temperature in the dark. The stop solution (50 ml) was added to each well. Finally, the result was obtained through a microplate reader at 450 nm.

Sample preparation and storage

Tissue homogenates

Cells have been rinsed in 0.01mol/l of ice-cold Phosphate Buffered Saline (PBS) (pH 7.0-7.2) and homogenized in 5–10 ml of PBS, followed by sonication or subjected to two freeze-thaw cycles. The homogenates were centrifuged for 5 minutes at 5,000 × g; the supernate and assay were removed or aliquoted and then stored at ≤ −86°C.

Calculation of the results

The results were recorded by determining the average of the readings for standard and control samples and then subtracting the standard optical density (OD) average zero. The standard curve was constructed by plotting the mean OD and concentration. Then, the best fit curve was drawn, and a standard curve was created. In the case of sample dilution, the concentration read from the standard curve has to be multiplied by the dilution factor.

Molecular docking study

The crystal structure of the active site complexed with a reference inhibitor was obtained. Water and inhibitor molecules were removed, and hydrogen atoms were added. The optimized 3D structures of molecules were subjected to generate different poses of compounds. The pose generated was rescored using the London dG scoring function. The poses generated were refined with the MMFF94 × force field. The best ten binding poses were analyzed after allowing auto-rotatable bonds to achieve the best score (Ali and El-Molla, 2019).

RESULTS AND DISCUSSION

Analytical data

The stoichiometries of the isolated complexes with H_2L are displayed in Table 1, and the proposed structure of ligand and different metal salts of Cr(III), Fe(III), and Co(II) produces complexes is shown in Figure 1. The molar conductivities of the complexes in DMF solution (10^{-3}M) are listed in Table 1. All complexes are nonelectrolytes except Cr(III) complex is an electrolyte (Mahmoud *et al*., 2015).

Nuclear magnetic resonance spectroscopy

The ^{1}H-NMR spectrum of thiosemicarbazide has been recorded as a d_6-DMSO solution (Fig. 2). The amide N(4)H linked to the Ph group was detected within the spectral region of 8.1 ppm, indicating the absence of H-bonding with d_6-DMSO agreeing with previous studies. The ^{1}H peak attributed to [N(1)H and N(2)H] was displayed at 9.8 and 9.2 ppm revealing the isolation of involvement of the hydrogens bonding with a combination of neutral and anionic ligands. The singlet at 3.3 and 3.2 ppm and the multiplet at 6.7–7.5 ppm were attributed to the CH_2 and aryl signals, respectively (Aly *et al*., 2021).

Mass spectroscopy

The mass spectrum of the ligand exhibited a molecular ion peak at m/z = 336 amu (Calc. m/z = 334.5). The major

Table 1. Analytical and physical data for the ligand H_2L, Cr(III), Fe(III), and Co(II) complexes.

Found (calc.) %				A m Ω^{-1} cm^2 mol^{-1}	M. Wt.	Compound (empirical formula)
M	N	H	C			
-	16.47 (16.73)	4.46 (4.48)	53.43 (53.81)	-	334.50	H_2L $C_{15}H_{15}ClN_4OS$
5.81 (5.95)	12.71 (12.82)	3.98 (4.15)	73.83 (73.97)	83	874.06	$[Cr(H_2L)_2Cl_2]ClEtOH$
9.58 (9.70)	9.59 (9.73)	4.06 (4.20)	31.15 (31.29)	25	575.79	$[Fe(H_2L)(OH)SO_4(H_2O)_2]2H_2O$
7.29 (7.36)	14.68 (14.77)	3.89 (4.12)	47.32 (47.51)	30	758.50	$[Fe(HL)_2(OH)]H_2O$
5.36 (5.43)	15.34 (15.50)	4.82 (5.02)	50.71(50.95)	18	1084.48	$[Co(H_2L)(HL)_2]1/2EtOH$

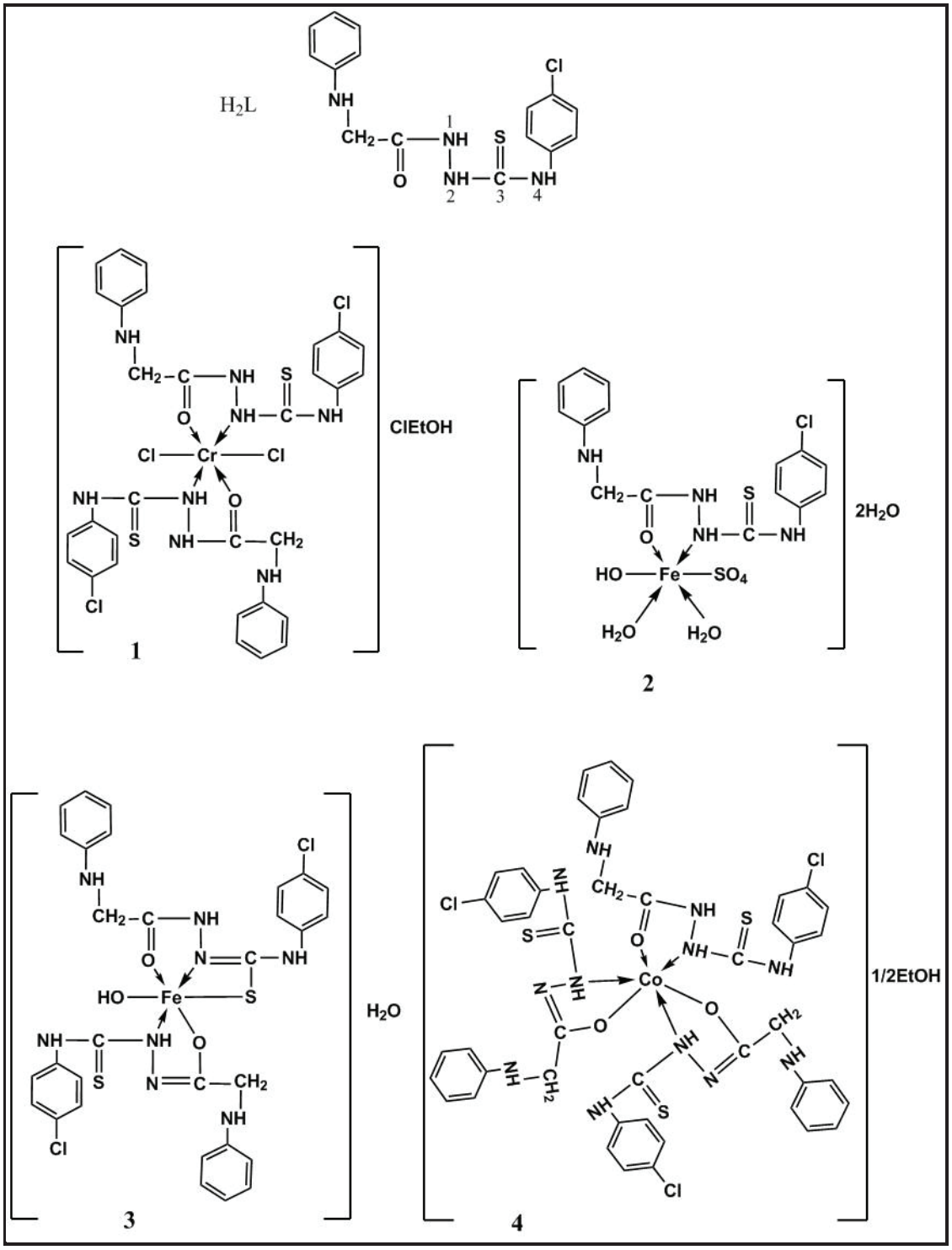

Figure 1. The proposed structure of ligand and its complexes.

fragment ions appear at m/z = 77, 112, 127, 201, 228.5, 259, and 336 for $[C_6H_4\text{-}3H]^+$, $[C_6H_5Cl\text{-}H]^+$, $[C_6H_5NCl\text{-}2H]^+$, $[C_7H_9N_3SCl]^+$, $[C_8H_9N_3SOCl\text{-}H]^+$, $[C_9H_{10}N_4OSCl\text{-}2H]^+$, and $[C_{15}H_{15}N_4OSCl]$, respectively (Fig. S1).

^{13}CNMR spectra

^{13}CNMR (δ, ppm): 58.3 (NCH_2); 113.5, 113.5, 117.8, 129.8, 129.8, 147.6 (Ph-C); 127.9, 127.9, 129.8, 129.8, 130.3, 135.6 (Cl-Ph-C); 170.7 (C=O); 181.5 (C=S) (Figure 3).

FTIR spectra

FTIR spectra of ligand

The significant absorptions of the functions incorporated in the ligand were recorded in the range of 400–4000 cm^{-1}, as presented in Table 2 (Abdalla *et al*., 2021). The intense absorption bands appeared at 1,673 and 752 cm^{-1} for υ(C=O) and υ(C=S), respectively, as shown in Table 2 and Figure 3. The absence of the —OH or —SH signals in the related NMR of the free ligand indicated the keto form of such ligand. The spectra of υ(N4-H),

υ(N2-H), and υ(N1-H) were detected at 3,335, 3,301, and 3,100 cm^{-1}, respectively.

FTIR spectra of Cr(III), Fe(III), and Co(II) complexes

The fundamental infrared bands which provide the structural evidence for the nature of the organic ligand binding to the ions are shown in Table 2, Figure 4, and Figures S2 and S3. The hydrate water molecules have been omitted from Table 2 for convenience. The coordination sites were identified by comparing ligand and complex spectra. Moreover, the infrared spectra of $[Cr(H_2L)_2Cl_2]ClEtOH$, $[Fe(HL)_2(OH)]H_2O$, $[Fe(H_2L)(OH)SO_4(H_2O)_2]2H_2O$, and $[Co(H_2L)(HL)_2]1/2EtOH$ showed that the ligand acts as neutral tetradentate, bidentate, or monobasic tridentate, coordinating with the C=O, ν(N2-H) group, and (C-S) resulting in a five-membered ring incorporating metal atom. However, νN(4)H remained at the same frequency or slightly shifted in position. In Cr(III) complex, νN(2)H shifted to low-frequency complexes (3 and 4) even in complexity. The appearing absorption spectra (621–504 and 459–416 cm^{-1}) attributed to ν(M-O) and ν(M-N), respectively (Al-Farhan *et al*., 2021). Hydroxo of complexes (2 and 3) revealed a broad strong band at 3,449–3,404 cm^{-1} for ν(OH) (Abdel-Rahman *et al*., 2021). For complex (3), a new band appeared at 1,018 cm^{-1} and was assigned to the monocoordinated sulfate group.

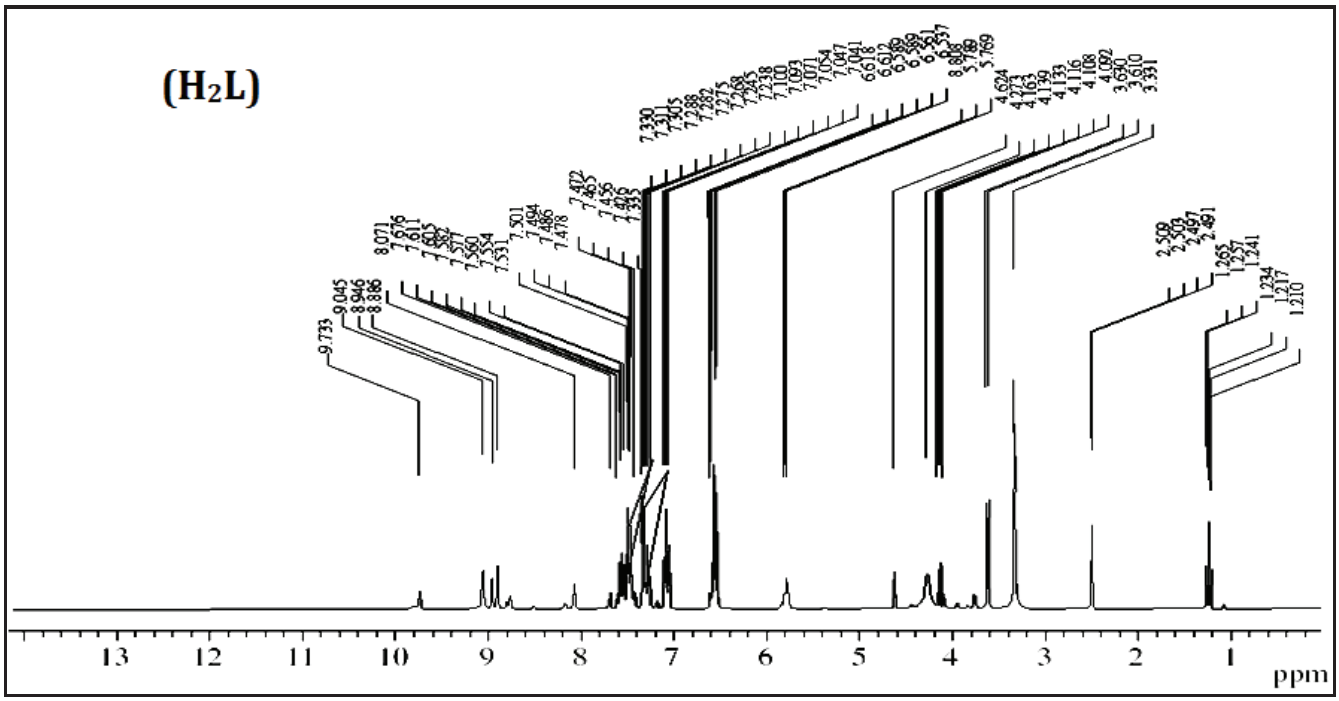

Figure 2. ^{1}H NMR spectra of ligand (H_2L) in DMSO-d_6 solution.

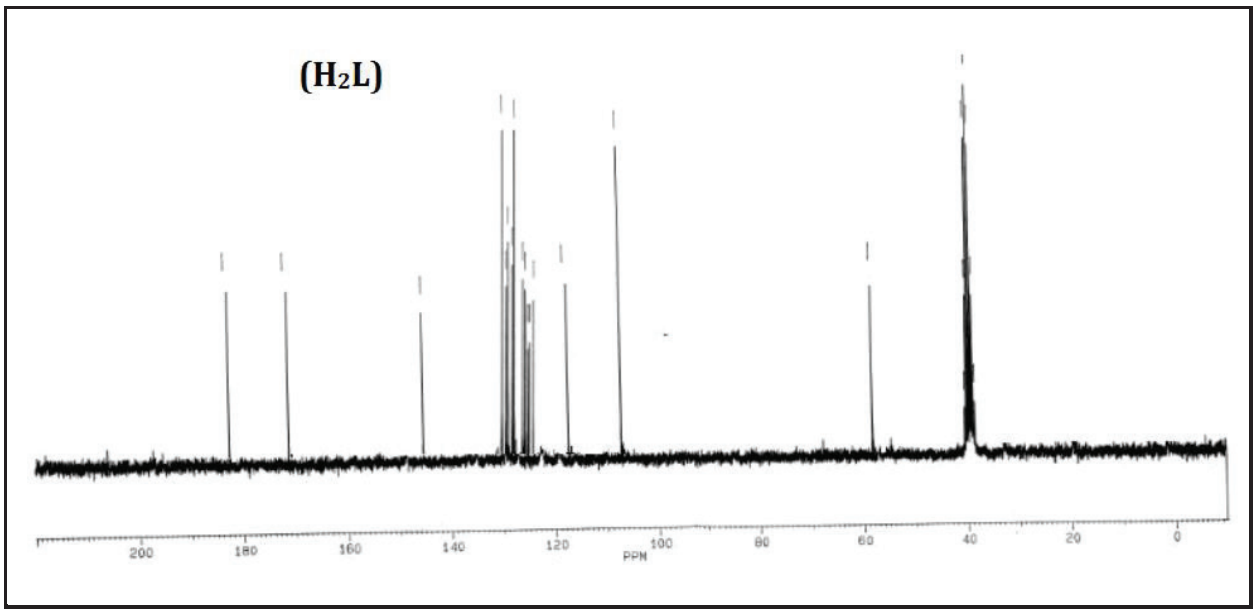

Figure 3. ^{13}C NMR spectra of ligand (H_2L) in DMSO-d_6 solution.

Electronic spectra and magnetic moment

The electronic spectral data are presented in Table 3. The ligand transitions were recorded at 245 and 300 nm for π-π* and n-π* transitions.

Cr(III) complexes

Cr(III) complex spectra have been recorded in regions of 335 and 362 nm, which were assigned to the octahedral geometry (Abdel-Rahman *et al*., 2021). In addition, the magnetic moment of the complex was 2.49 B.M.

Fe(III) complexes

Fe(III) complexes (2 and 3) spectra have been recorded in DMF solution in regions 320 and 550 as well as 280, 295, and 440 nm, respectively, attributed to the octahedral geometry (Darari *et al*., 2020). The r.t. magnetic moments of complexes (2 and 3) were 5.0 and 4.8 B.M., respectively.

Co(II) complexes

Co(II) complex(4) spectra revealed bands in the visible region at 600 and 305 nm attributed to $^4T_{1g}(F) \rightarrow {}^4A_{2g}$ (F) and $^4T_{1g}(F) \rightarrow {}^4T_{1g}$ (P) transition showing an octahedral conformation (Shebl *et al*., 2010). Also, the r.t. magnetic moment was 4.2 B.M.

Thermal studies thermogravimetric and derivative thermogravimetry (TG/DTG)

The thermal properties of the ligand for Fe(III) and Co(II) complexes were performed by thermogravimetric analysis (TG/DTG) under a nitrogen atmosphere with a temperature range of 25–800°C (Table 4).

Table 2. Infrared spectral bands (cm^{-1}) for ligand (H_2L), Cr(III), Fe(III), and Co(II) complexes.

No.	Compounds	*v*(OH)/EtOH *v*(N_4-*H*)	ν(N2-H)	ν(N1-H)	ν(C=O)	ν(C=S)	ν(M-O)	ν(M-N)
	H_2L	3,335	3,302	3,100	1,670	750	—	—
1	$[Cr(H_2L)_2Cl_2]ClEtOH$	3,410	3,100	3,306	1,666	752	504	416
2	$[Fe(H_2L)(OH)SO_4(H_2O)_2]2H_2O$	3,449 3,376	3,321	3,200	1,665	749	621	446
3	$[Fe(HL)_2(OH)]H_2O$	3,404 3,294	—	3,150	1,673 1,632	752	568	447
4	$[Co(H_2L)(HL)_2]1/2EtOH$	3,408 3,294	—	3,155	1,672	752	563	459

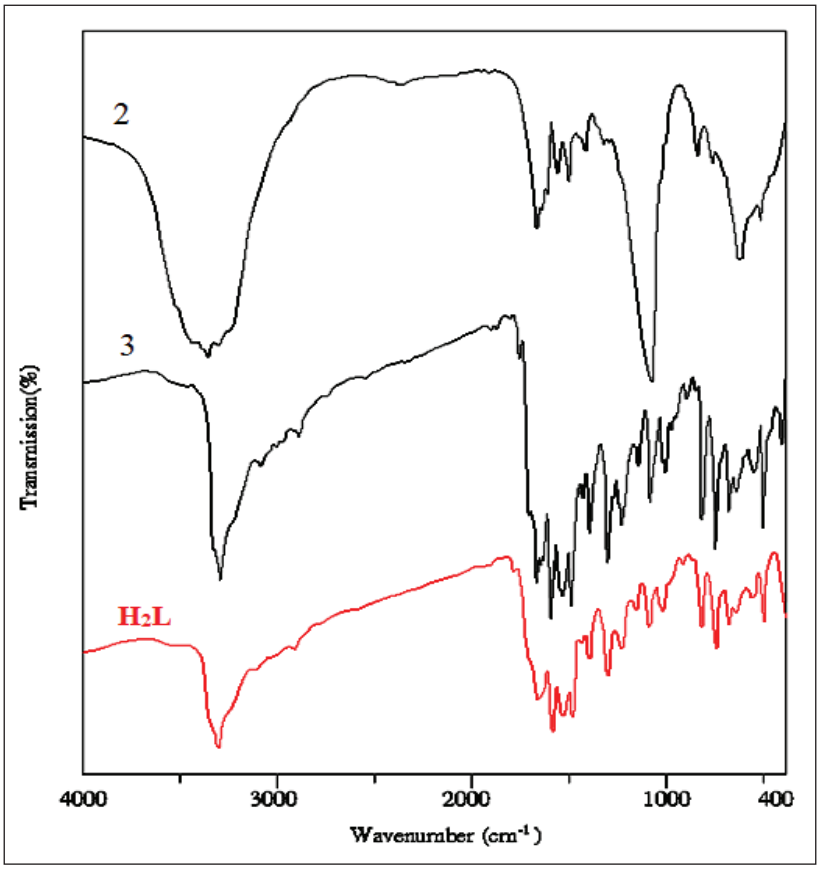

Figure 4. FTIR spectra of the ligand (H_2L) and Fe(III) complexes (2 and 3).

Table 3. Magnetic moment and electronic spectral data for ligand, Cr(III), Fe(III), and Co(II) complexes.

No.	Compounds	λ_{max} (nm)	$\mu_{eff\ (B.M)}$
	H_2L	245 300	—
1	$[Cr(H_2L)_2Cl_2]ClEtOH$	335 362	2.49
2	$[Fe(H_2L)(OH)SO_4(H_2O)_2]2H_2O$	320 550	5.0
3	$[Fe(HL)_2(OH)]H_2O$	280 295 440	4.8
4	$[Co(H_2L)(HL)_2]1/2EtOH$	310 600	4.2

Table 4. Thermal data for ligand, Fe(III), and Co(II).

Complex	Temp. range /°C thermo gravimetric analysis (TGA)	Calc. Wt. loss % (F.)	Assignments
H_2L	189 190–633	100 (99.9)	Melting decomposition
$[Cr(H_2L)_2Cl_2]ClEtOH$ Residue	23–149 149–294 294–408 At 408	8.25 (7.91) 46.53 (46.71) 39.27 (39.45) 5.89)5.94)	$EtOH+C_2H_2$ Decomposition Decomposition Cr
$[Fe(H_2L)(OH)SO_4(H_2O)_2]2H_2O$ Residue	27–153 153–489 At 799	12.5 (12.4) 57.2 (57.8) 30.3 (29.8)	$4H_2O$ Decomposition 2FeO + CO
$[Fe(HL)_2(OH)]H_2O$ Residue	32–158 158–550 At 700	2.2 (2.4) 91.5 (91.3) 6.9 (7.4)	H_2O Decomposition Fe
$[Co(H_2L)(HL)_2]1/2EtOH$ Residue	24–154 154–438 At 800	2.2 (2.1) 79.5 (78.9) 18.3 (19.0)	½ EtOH Decomposition 2CoO + 2CO

Ligand

The TG curve of the ligand showed that the ligand was thermally stable up to 189°C followed by the melting point at 190°C (Fig. 5a). Additionally, the curve revealed that the decomposition step occurred in a temperature range of 190°C–633°C, accompanied by a total mass loss of 100% (Found 100%).

Cr(III) complexes

TG curves of Cr(III) complex (1) showed four decomposition steps in a temperature range of 23°C–149°C (Calc./Found % 8.25/7.91) (Fig. S4). In addition, it was designated to dissolve an ethanol molecule and a C_2H_2 moiety. In the first and second steps, the TG curve showed that the complex gradually decomposed at a temperature range between 149°C and 408°Cand ended with the formation of Cr associated with DTG peaks at 234°C, 320°C, and 379°C.

Fe(III) complexes

TG curves of Fe(III) complexes indicated the mass loss in temperature ranges of 32°C–158°C and 27°C–153.6°C (Calc./Found % 2.4/2.2.; 12.4/12.5), respectively, besides DTG peaks at 33°C and 94.6°C, assigned for releasing one and four water molecules of crystallization and coordination (complexes 2 and 3). The TG showed a gradual decomposition at 158°C–550°C and 153.6°C–489°C, leading to the formation of the metal complex (2), metal oxide, and CO in complex (**2**) (Fig. 5b and c).

Co(II) complexes

The TG curves of Co(II) complex (4) are presented in Figure 5d. The data revealed that the mass loss was in the temperature range of 24°C–153.8°C (Calc./Found % 2.2/2.1), respectively, with DTG peak at 31°C assigned to the desolation of a half molecule of the solvent. Also, complex (4) was gradually decomposed at 154°C–438°C resulting in the formation of metal oxide and CO.

Biological activities

Antibacterial activities

The dose-dependent pattern of Cr(III), Fe(III), and Co(II) complexes and their corresponding legends showed remarkable activities (Table 5). For the concentrations of 1, 5, and 7 µg/ml of ligand, Cr(III), Fe(III), and Co(II) complexes, the antibacterial activity was tested against *E. coli* and *S. pyogenes* as represented in Figure 6. The results were found as follows: the antibacterial activity of the complexes > ligand for the two bacterial species, where the Co(II) complex was the highest one among them. According to the results, in the case of complexes, the role of chelation in facilitating the cross-potency into the cell membrane of *E. coli* can be explained by Tweedy's chelation theory (Abdalla *et al*., 2020; Fathima *et*

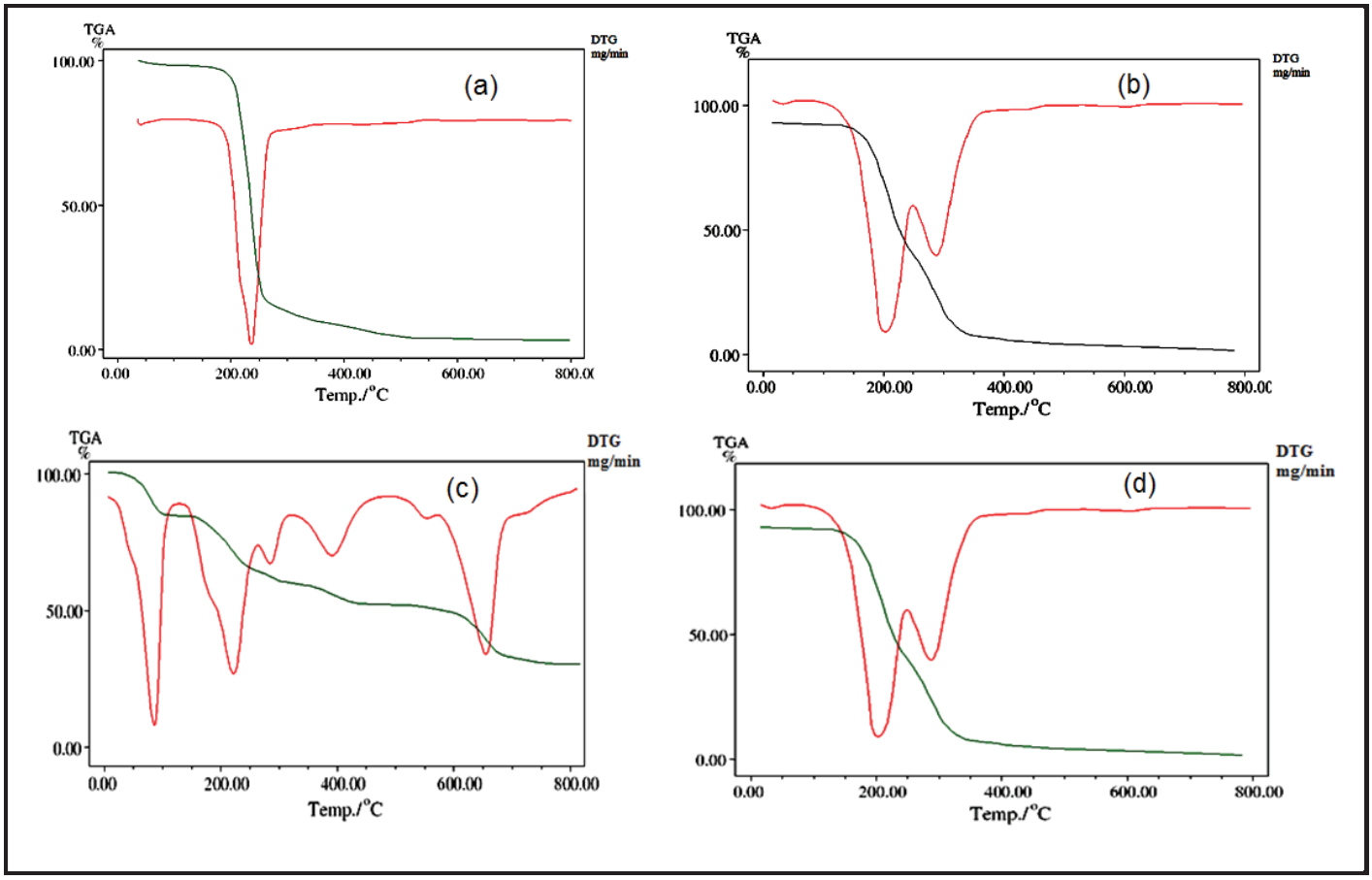

Figure 5. a. TGA/ DTG curves of the ligand (H_2L). b. TGA/ DTG curves of the complex [Fe $(HL)_2(OH)]H_2O$. c. TGA/ DTG curves of the complex [$Fe(H_2L)(OH)SO_4(H_2O)_2$]2 H_2O. d. TGA/ DTG curves of the complex [$Co(H_2L)(HL)_2$]1/2 EtOH.

Table 5. Antibacterial activities of ligand, Cr(III), Fe(III), and Co(II) complexes against *E. coli and S. pyogenes*.

No.	Compound	Inhibition% *E. coli*			Inhibition% *S. pyogene*		
		7 mg	5 mg	1 mg	7 mg	5 mg	1 mg
	H_2L	94	91.66	59.66	96	94.23	82.50
1	$[Cr(H_2L)_2Cl_2]$ ClEtOH	94.53	93.72	89.52	97.63	95.16	86.23
2	Fe (H_2L) $(OH)SO_4(H_2O)_2.2$ H_2O	70.01	68.25	57.64	88.15	85.42	71.86
3	Fe $(HL)_2(OH).H_2O$	95.52	92.19	87.52	97.58	96.66	85.42
4	Co (H_2L) $(HL)_2.1/2$ EtOH	95.24	93.42	90.89	98.29	95.18	90.72

al., 2020). Chelation/complication has the potential to induce the lipophilic character of the central metal, thus favoring its penetration through the lipid layer of the cell membrane**.** In the instance of *S. pyogenes* (gram +), the complex was effective at concentrations of 1, 5, and 7 µg/ml. It was noticed that the incorporation of certain moieties, such as N(2)H linkage, introduced into such compounds, enhanced their bioactivity (Singh *et al*., 2013). Furthermore, the results reflected that the observed activity may allow such compounds as potential drugs against pathogenic bacterial diseases.

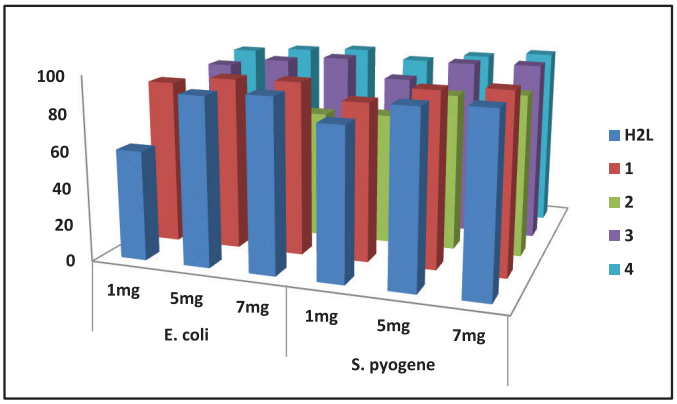

Figure 6. *In vitro* antibacterial activities of ligand, Cr(III), Fe(III), and Co(II) complexes against *E. coli* and *S. pyogenes.*

Antitumor activity of ligand, Fe(III), and Co(II) complexes

Determining SOD activity

Cancer is a major cause of morbidity and mortality worldwide. Scientific evidence revealed that oxidative stress

(OS) was related to cancer because it is associated with the existence of increased reactive oxygen species. Moreover, it was believed to be associated with DNA, proteins, and lipids damage, thus initiating carcinogenesis resulting in cancer development, and characterized by altered intracellular redox homeostasis (Vera-Ramirez *et al*., 2011). Additionally, carcinogenesis was proposed to be indicated by lower expression or low antioxidant enzyme activity (Sharma *et al*., 2009).

In this study, all compounds (H_2L, Fe(III), and Co(II)) were investigated regarding the antioxidant enzyme status, which was elucidated by measuring SOD activities by their OD and concentration of all tested compounds. The concentration and of SOD in the tested compounds are presented in Table 6, where the OD of ligand was 0.785 (Fig. 7a) and their concentration was 1.357 mg/ml, while the OD of Fe(III) and Co(II) complexes was 0.695 and 0.959 (Fig. 7b and c)**,** and their concentration was 1.164 and 1.77, *respectively.*

Cells of ligand and metal complexes

The antioxidant status has been noted as the first investigation of Co(II) and Fe(III) complexes' effects on the treatment of MCF7 cells. In addition, the SOD levels were elevated in the Co complex compared to that of Fe (Fig. 8 and Table 6), which could be due to the OS under which the cancer cells were exposed. The antioxidants were always detoxifying or scavenging free radicals, which leads to lowering the levels of the intracellular antioxidant enzyme. Similarly, the data revealed that the antioxidant enzymes SOD and catalase were elevated in normal cells compared to cancer cells (Khan *et al*., 2015). Hydrogen peroxide has been widely used as an OS catalyst in various *in vitro* studies (Hwang and Yen, 2008)**.** There are hypothetical studies to increase cell proliferation at low levels of exogenous H_2O_2 while inducing OS and cytotoxic effects on cells at higher concentrations (Kim *et al*., 2001).

Due to their potentially beneficial pharmacological properties and the great diversity of bonding patterns and stereochemistry, the synthesis and the structural investigations of thiosemicarbazone and related metal complexes have received much interest (Mishra *et al*., 2006). This work showed a strong antibacterial behavior of Cr(III), Fe(III), and Co(II) complexes in comparison with the ligand. In line with a similar study in the last two decades, these compounds have emerged as important sulfur-containing ligands (Dutta *et al*., 2002). The broad spectra of biological properties based on the parent aldehyde or ketones, such as antitumor (Afrasiabi *et al*., 2004), antibacterial, and antifungal (Agarwal *et al*., 2006; Singh and Singh, 2001), and their physicochemical effects (Labisbal *et al*., 2003) are the driving force behind the coordination chemistry. Furthermore, due to their cytotoxic effect, their medicinal properties have been examined. They also maintain unusual oxidation states and produce a distinct oxidation state making them very potent antibiological and sterilizing drugs.

Table 6. Antitumor activity of ligand, Fe(III), and Co(II) complexes.

Sample ID	SOD	
	OD	Conc. (mg/ml)
H_2L	0.785	1.3 57
Fe complex (3)	0.695	1.164
Co complex (4)	0.959	1.77

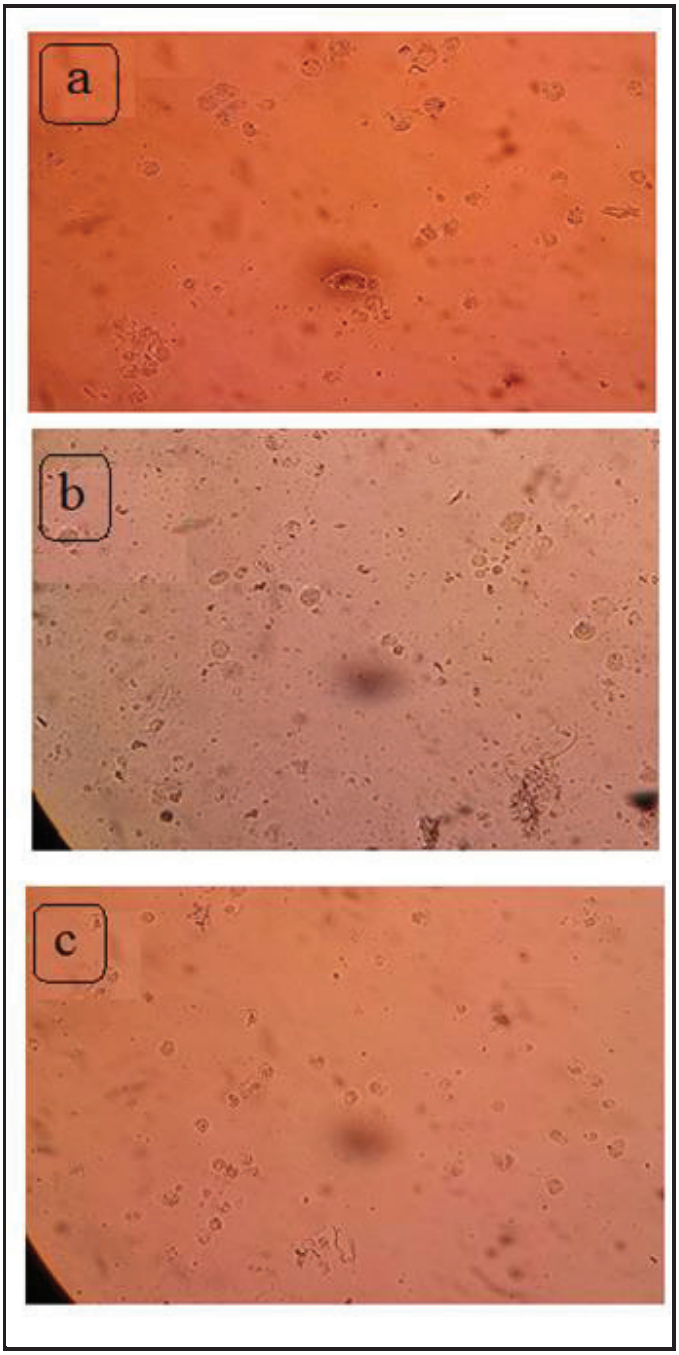

Figure 7. (a–c). Cancer cell after treatment with ligand (a), Fe(III) (b), and Co(II) (c) complexes.

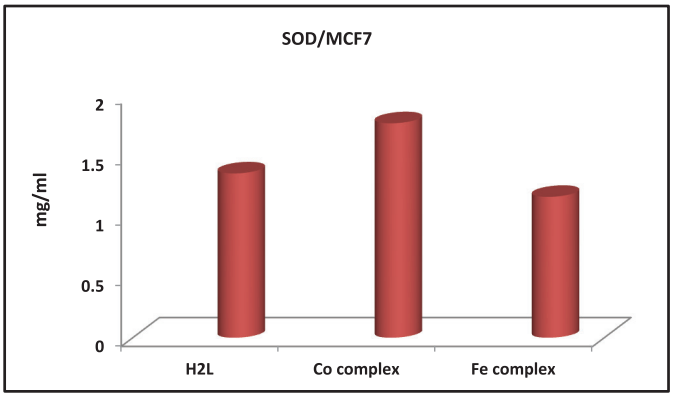

Figure 8. Antitumor activity of ligand and Co(II) and Fe(III) complexes.

Table 7. Binding affinity of complexes against ribosyl transferase (code: 3GEY).

Docking 3GEY			
Compound	**Scoring energy (RMSD) Kcal/mol**	**Involved amino acids**	**Type of interaction**
H_2L	−4.53 (1.60)	Asp-*A*623, Leuc-*A*624, and Lys-*A*518 and His-*B*550	Side chain acceptor, backbone donor, and arene-cation interaction
1 Cr (1)	−3.37 (1.38)	Solvent contact	
2 Fe (2)	−3.94 (1.38)	Asp-A626, Ly-A525, and Ly-A525	Side chain donor and side chain acceptor
3 Fe (3)	−6.53 (2.84)	Thr-A622	Side chain acceptor
4 Co (4)	−6.33 (2.17)	Asp-*A*623 and Ly-*A*616	Side chain acceptor and arene-cation interaction

(1) [Cr(H2 L)2 Cl2]Cl.EtOH.
(2) [Fe(H2 L)(OH)SO4 (H2 O)2].2H2 O.
(3) [Fe(HL)2 (OH)].H2 O.
(4) [Co(H2 L)(HL)2].1/2EtOH.

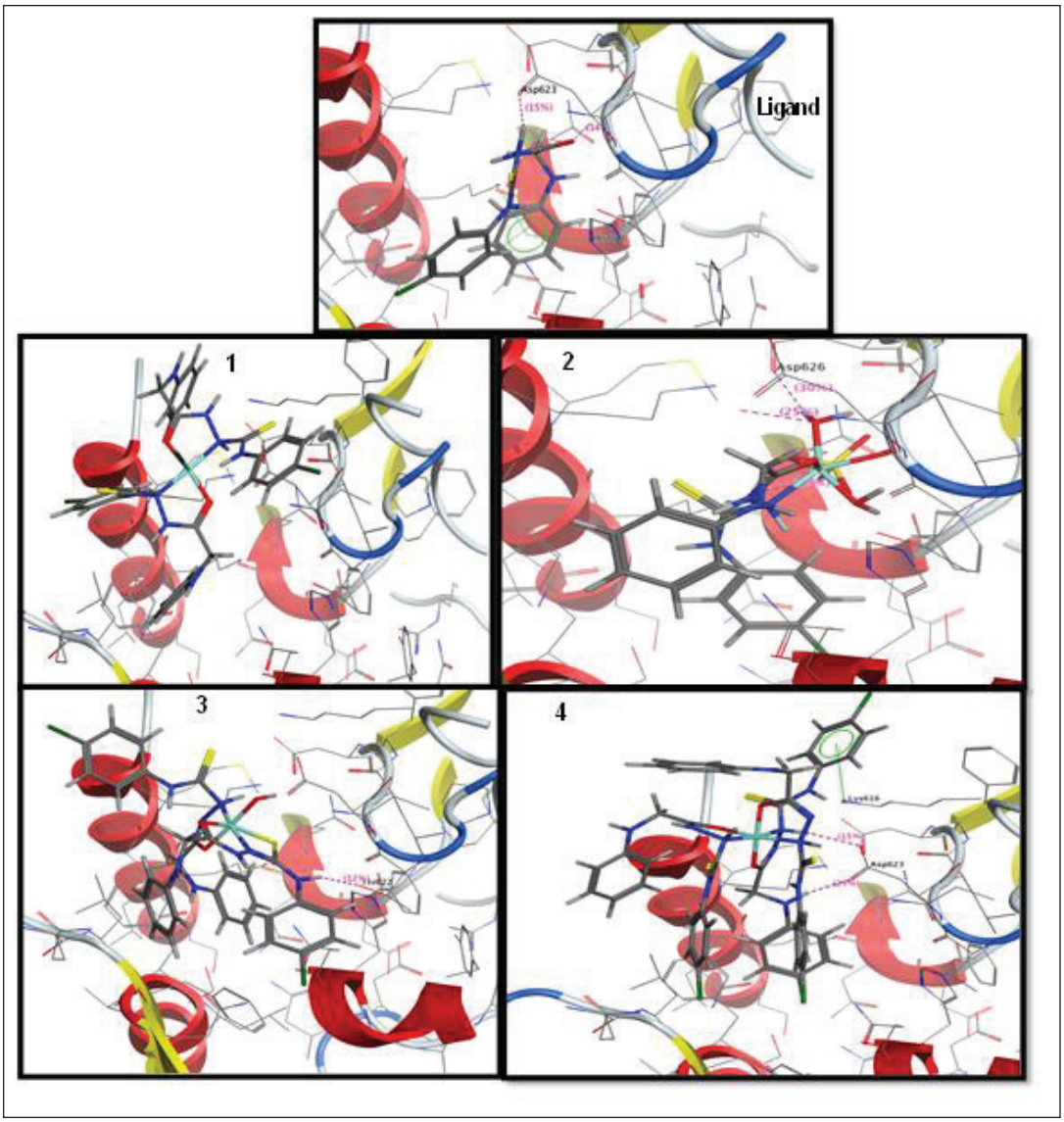

Figure 9. 3D binding affinity of compounds ligand and complexes1–4, respectively, against ribosyltransferase (PDB ID).

Molecular modeling and analysis of the docked results

The *in vitro* results of the antibacterial activities are presented in Table 7. The obtained outcomes may be attributed to the coincidental formation of *H*-bonds by toxophoric groups (–C=O and NH) with the active cell center constituents, which leads to significant overlap with the normal cell (Al-Farhan *et al*., 2021). In addition, being an important functional center, the amino ($SO4^{2-}$) and oxygen water molecules are active participants, as shown in the docking results (Fig. 9). Table 7 presents the results and the corresponding amino acid interactions

of the docked compounds. The complexes and their ligand precursors revealed interesting interactions with the amino acids of the ribosyltransferase active site (code: 3GEY) as a side chain acceptor, backbone donor, and arene-cation interaction. The –NH– group promoted a binding interaction with Asp-*A*623 in both ligand and complex (4), Asp-*A*626 and Thr-*A*622, complex (2), and complex (3), respectively. Additionally, we have Asp-*A*623 in OCET, NOCET, Rh–OCET, Rh–BOCET, and Rh-NOCET, respectively. Moreover, the oxygen of the carbonyl group in the ligand interacted with the Leu-624 amino acid. On the other hand, the oxygen of the involved H_2O molecule forms a hydrogen bond with Lys-A525 in complex (2). In addition, there are interactions of arene-cation with Lys-A518 and Lys-A616 in both ligands and their complexes (4). Accordingly, an agreement was observed with the molecular dockings of the selected enzyme target. However, complex (2) showed the lowest zone inhibition value in both microorganisms and theoretically low scoring value. Also, complexes 4 and 3 showed the highest antibacterial effect with the highest recorded energy values.

CONCLUSION

To conclude, this study focused on the biological applications and molecular docking of four new complexes of $[Cr(H_2L)_2Cl_2]ClEtOH$, $[Fe(H_2L)\ (OH)SO_4(H_2O)_2]2H_2O$, $[Fe(HL)_2(OH)]H_2O$, and $[Co(H_2L)(HL)_2]1/2EtOH$. The complexes were evaluated for their biological activities as antibacterial and anticancer compounds. All the new complexes showed significant antibacterial activity against two members of the most pathogenic bacteria (*E. coli* and *S. pyogenes*). Activities were investigated as follows: complexes > ligand against the two bacterial species, with the highest values for Co(II) complex. *In vitro* cytotoxicity of the complexes indicated that the complexes exhibited a potent cytotoxic activity. The super complex had anticancer efficacy against MCF-7 compared to the free ligand. Furthermore, they have also retained unusual oxidation states, making them very promising antibiotics and sterilizers. The affinity patterns towards the amino acids in the active site of ribosyltransferase (code: 3GEY) were shown by hydrogen bond formation and interaction. Consequently, the present findings provide an opportunity to develop and discover novel antimicrobials and thus counteract the growing resistance.

LIST OF ABBREVIATIONS

H2L: Ligand; Complex 1: $[Cr(H_2L)_2Cl_2]ClEtOH$; Complex 2: $[Fe(H_2L)(OH)SO_4(H_2O)_2]2H_2O$; Complex 3: $[Fe(HL)_2(OH)]H_2O$; Complex 4: $[Co(H_2L)(HL)_2]1/2EtOH$; BHI, Brain heart infusion; DMF, Dimethylformamide; DMSO, Dimethylsulfoxide; DTG, Derivative thermogravimetry; NB, Nutrient broth; OD, Oxoaporphine derivative; OS, Oxidative stress; PBS, Phosphate buffered saline; ROS, Reactive oxygen species; SOD, Superoxide dismutase; TG, Thermogravimetric

AUTHOR CONTRIBUTIONS

All authors made substantial contributions to conception and design, acquisition of data, or analysis and interpretation of data; took part in drafting the article or revising it critically for important intellectual content; agreed to submit to the current journal; gave final approval of the version to be published; and agree to be accountable for all aspects of the work. All the authors are eligible to be an author as per the international committee of medical journal editors (ICMJE) requirements/guidelines.

FINANCIAL SUPPORT

There is no funding to report.

CONFLICTS OF INTEREST

The authors report no financial or any other conflicts of interest in this work.

ETHICAL APPROVALS

This study does not involve experiments on animals or human subjects.

DATA AVAILABILITY

All data generated and analyzed are included in this research article.

PUBLISHER'S NOTE

This journal remains neutral with regard to jurisdictional claims in published institutional affiliation.

REFERENCES

Abdalla EM, Rahman LHA, Abdelhamid AA, Shehata MR, Alothman AA, Nafady A. Synthesis, characterization, theoretical studies, and antimicrobial/antitumor potencies of salen and salen/imidazole complexes of Co (II), Ni (II), Cu (II), Cd (II), Al (III) and La (III). Appl Organomet Chem, 2020; 34(11):e5912; doi: 10.1002/aoc.5912.

Abdalla EM, Hassan SS, Elganzory HH, Aly SA, Alshater H. Molecular docking, DFT calculations, effect of high energetic ionizing radiation, and biological evaluation of some novel metal (II) heteroleptic complexes bearing the thiosemicarbazone ligand. Molecules, 2021; 26(19):5851; doi.org/10.3390/molecules26195851.

Abdel-Rahman LH, Basha MT, Al-Farhan BS, Shehata MR, Abdalla EM. Synthesis, characterization, potential antimicrobial, antioxidant, anticancer, DNA binding, and molecular docking activities and DFT on novel Co (II), Ni (II), VO (II), Cr (III), and La (III) schiff base complexes. Appl Organomet Chem, 2021; 36(1):e6484; doi: 10.1002/aoc.6484.

Afrasiabi Z, Sinn E, Chen J, Ma Y, Rheingold AL, Zakharov LN, Rath N, Padhye S. Appended 1, 2-naphthoquinones as anticancer agents 1: synthesis, structural, spectral and antitumor activities of ortho-naphthaquinone thiosemicarbazone and its transition metal complexes. Inorgan Chim Acta, 2004; 357(1):271–78; doi:10.1016/S0020-1693(03)00484-5

Agarwal RK, Singh L, Sharma DK. Synthesis, spectral, and biological properties of copper (II) complexes of thiosemicarbazones of schiff bases derived from 4-aminoantipyrine and aromatic aldehydes. Bioinorgan Chem Appl, 2006; 2006:10; doi.org/10.1155/BCA/2006/59509.

Akhurst RJ. Antibiotic activity of *Xenorhabdus* spp., bacteria symbiotically associated with insect pathogenic nematodes of the families *Heterorhabditidae* and Steinernematidae. Microbiology, 1982; 128:3061–65; doi: 10.1099/00221287-128-12-3061.

Al-Farhan BS, Basha MT, Rahman LHA, El-SaghierAMM, El-Ezz DA, Marzouk AA, Shehata MR, Abdalla EM. Synthesis, DFT calculations, antiproliferative, bactericidal activity and molecular docking of novel mixed-ligand salen/8-hydroxyquinoline metal complexes. Molecules, 2021; 26(16):4725; doi.org/10.3390/molecules26164725.

Ali IO, El-Molla M. Synthesis of zinc oxide and silver/zinc oxide nanocomposite for production of antimicrobial textiles. Egypt J Chem, 2019; 62:797–817; doi: 10.21608/ejchem.2019.17392.2083

Aly SA, Elganzory HH, Mahross MH, Abdalla EM. Quantum chemical studies and effect of gamma irradiation on the spectral, thermal, X-ray diffraction and DNA interaction with Pd (II), Cu (I), and Cd (II) of hydrazone derivatives. Appl Organomet Chem, 2021; 35(4):e6153; doi: 10.1002/aoc.6153.

Aly S, El-Boraey HA. Effect of gamma irradiation on spectral, XRD, SEM, DNA binding, molecular modling and antibacterial property of some (Z) N-(furan-2-yl) methylene)-2-(phenylamino) acetohydrazide metal (II) complexes. J Mol Struct, 2019; 1185:323–32; doi.org/10.1016/j.molstruc.2019.02.069.

Arnold AR, Grodick MA, Barton JK. DNA charge transport: from chemical principles to the cell. Cell Chem Biol, 2016; 23(1):183–97; doi: 10.1016/j.chembiol.2015.11.010.

Basha MT, Rodríguez C, Richardson DR, Martínez M, Bernhardt PV. Kinetic studies on the oxidation of oxyhemoglobin by biologically active iron thiosemicarbazone complexes: relevance to iron-chelator-induced methemoglobinemia. J Biol Inorg Chem, 2014; 19(3):349–57; doi: 10.1007/s00775-013-1070-9.

Darari M, Francés-Monerris A, Marekha B, Doudouh A, Wenger E, Monari A, Haacke S, Gros PC. Towards iron (II) complexes with octahedral geometry: synthesis, structure and photophysical properties. Molecules, 2020; 25(24):5991; doi.org/10.3390/molecules25245991.

De Oliveira JF, da Silva Al, Vendramini-Costa DB, da Cruz Amorim CA, Campos JF, RibeiroAG, de Moura RO, Neves JL, Ruiz ALTG, de Carvalho JE, de Lima MDCA. Synthesis of thiophene-thiosemicarbazone derivatives and evaluation of their in vitro and in vivo antitumor activities. Eur J Med Chem, 2015; 104:148–56; doi.org/10.1016/j.ejmech.2015.09.036.

Dutta S, Basuli F, Peng SM, Lee GH, Bhattacharya S. Synthesis, structure and redox properties of some thiosemicarbazone complexes of rhodium. New J Chem, 2002; 26(11):1607–12; doi.org/10.1039/B205338C

Fathima SSA, Meeran MMS, Nagarajan ER. Synthesis, characterization and biological evaluation of novel 2, 2′-((1, 2-diphenylethane-1, 2-diylidene) bis (azanylylidene)) bis (pyridin-3-ol) and metal complexes: molecular docking and in silico ADMET profile. Struct Chem, 2020; 31(10):521–39; doi: 10.1007/s11224-019-01425-7.

Fuss JO, Tsai CL, Ishida JP, Tainer JA. Emerging critical roles of Fe–S clusters in DNA replication and repair. Biochim Biophys Acta Mol Cell Res, 2015; 1853:1253–71; doi.org/10.1016/j.bbamcr.2015.01.018.

Garg BS, Jain VK. Analytical applications of thiosemicarbazones and semicarbazones. Microchem J, 1988; 38(2):144–69; doi.org/10.1016/0026-265X(88)90017-3.

Grodick MA, Muren NB, Barton Jk. DNA charge transport within the cell. Biochemistry, 2015; 54(4):962–73; doi.org/10.1021/bi501520w.

Hwang SL, Yen GC. Neuroprotective effects of the citrus flavanones against H2O2-induced cytotoxicity in PC12 cells. J Agric Food Chem, 2008; 56(3):859–64; doi.org/10.1021/jf072826r.

Jumina J, Harizal H. Dermatologic toxicities and biological activities of chromium, 2019; doi: 10.5772/intechopen.90347.

Kalinowski DS, Richardson DR. The evolution of iron chelators for the treatment of iron overload disease and cancer. Pharmacol Rev, 2005; 57(4):547–83; doi.org/10.1124/pr.57.4.2.

Khan T, Ahmad R, Joshi S, Khan AR. Anticancer potential of metal thiosemicarbazone complexes: a review. Der Chemica Sinica, 2015; 6(12):1–11.

Kim BY, Han MJ, Chung AS. Effects of reactive oxygen species on proliferation of Chinese hamster lung fibroblast (V79) cells. Free Radic Biol Med, 2001; 30(6):686–98; doi.org/10.1016/S0891-5849(00)00514-1.

Küçükgüzel G, Kocatepe A, De Clercq E, Şahin F, Güllüce M. Synthesis and biological activity of 4-thiazolidinones, thiosemicarbazides derived from diflunisal hydrazide. Eur J Med Chem, 2006; 41(3):353–59; doi.org/10.1016/j.ejmech.2005.11.005.

Labisbal E, Haslow KD, Sousa-Pedrares A, Valdés-Martínez J, Hernández-Ortega S, West DX. Copper (II) and nickel (II) complexes of 5-methyl-2-hydroxyacetophenone N (4)-substituted thiosemicarbazones. Polyhedron, 2003; 22(20):2831–37; doi.org/10.1016/S0277-5387(03)00405-4.

Lieu PT, Heiskala M, Peterson PA, Yang Y. The roles of iron in health and disease. Mol Asp Med, 2001; 22(1–2):1–87; doi.org/10.1016/S0098-2997(00)00006-6.

Lv J, Liu T, Cai S, Wang X, Liu L, Wang Y. Synthesis, structure and biological activity of cobalt (II) and copper (II) complexes of valine-derived schiff bases. J Inorg Biochem, 2006; 100(11):1888–96; doi.org/10.1016/j.jinorgbio.2006.07.014.

Mahmoud WH, Mahmoud NF, Mohamed GG, El-Sonbati AZ, El-Bindary AA. Synthesis, spectroscopic, thermogravimetric and antimicrobial studies of mixed ligands complexes. J Mol Struct, 2015; 1095:15–25; doi.org/10.1016/j.molstruc.2015.04.004.

Manikandan R, Anitha P, Prakash G, Vijayan P, Viswanathamurthi P, Butcher PJ, Malecki JG. Ruthenium (II) carbonyl complexes containing pyridoxal thiosemicarbazone and trans-bis (triphenylphosphine/arsine): synthesis, structure and their recyclable catalysis of nitriles to amides and synthesis of imidazolines. J Mol Catal A Chem, 2015; 398:312–24; doi.org/10.1016/j.molcata.2014.12.017.

Merlot AM, Kalinowski DS, Richardson DS. Novel chelators for cancer treatment: where are we now? Antioxid Redox Signal, 2013; 18(8):973–1006; doi.org/10.1089/ars.2012.4540.

Mishra D, Naskar S, Drew MGB, Chattopadhyay SK. Synthesis, spectroscopic and redox properties of some ruthenium (II) thiosemicarbazone complexes: structural description of four of these complexes. Inorgan Chim Acta, 2006; 359(2):585–92; doi: 10.1016/j.ica.2005.11.001

Murphy MB, Mercer SL, Deweese JE. Inhibitors and poisons of mammalian type II topoisomerases. Adv Mol Toxicol, 2017; 11:203–40; doi.org/10.1016/B978-0-12-812522-9.00005-1.

Nehar OK, Mahboub R, Louhibi S, Roisnel T, Aissaoui M. New thiosemicarbazone schiff base ligands: synthesis, characterization, catecholase study and hemolytic activity. J Mol Struct, 2020; 1204:127566; doi.org/10.1016/j.molstruc.2019.127566.

Palaska E, Şahin G, Kelicen P, Durlu NT, Altinok G. Synthesis and anti-inflammatory activity of 1-acylthiosemicarbazides, 1, 3, 4-oxadiazoles, 1, 3, 4-thiadiazoles and 1, 2, 4-triazole-3-thiones. Farmaco, 2002; 57(2):101–07; doi.org/10.1016/S0014-827X(01)01176-4.

Pandeya SN, Sriram D, Nath G, DeClercq E. Synthesis, antibacterial, antifungal and anti-HIV activities of schiff and mannich bases derived from isatin derivatives and N-[4-(4′-chlorophenyl) thiazol-2-yl] thiosemicarbazide. Eur J Pharm Sci, 1999; 9(1):25–31; doi.org/10.1016/S0928-0987(99)00038-X.

Paul VD, Lill R. Biogenesis of cytosolic and nuclear iron–sulfur proteins and their role in genome stability. Biochim Biophys Acta Mol Cell Res, 2015; 1853(6):1528–39; doi.org/10.1016/j.bbamcr.2014.12.018.

Pavon JMC, Sanchez JCJ, Pino F. The 4-phenyl-3-thiosemicarbazone of biacetylmonoxime as an analytical reagent. Spectrophotometric determination of manganese. Anal Chim Acta, 1975; 75(2):335–42; doi.org/10.1016/S0003-2670(01)85358-7.

Pechova A, Pavlata L. Chromium as an essential nutrient: a review. Vet Med, 2007; 52(1):1–18; doi: 10.17221/2010-VETMED.

Plech T, Wujec M, Siwek A, Kosikowska U, Malm A. Synthesis and antimicrobial activity of thiosemicarbazides, s-triazoles and their mannich bases bearing 3-chlorophenyl moiety. Eur J Med Chem, 2011; 46(1):241–48; doi.org/10.1016/j.ejmech.2010.11.010.

Prajapati NP, Patel HD. Novel thiosemicarbazone derivatives and their metal complexes: recent development. Synth Commun, 2019; 49(21):2767–804; doi.org/10.1080/00397911.2019.1649432.

Sartorelli AC, Moore EC, Zedeck MS, Agrawal KC. Inhibition of ribonucleoside diphosphate reductase by 1-formylisoquinoline thiosemicarbazone and related compounds. Biochemistry, 1970; 9(23):4492–98; doi.org/10.1021/bi00825a005.

Sharma A, Tripathi M, Satyam A, Kumar L. Study of antioxidant levels in patients with multiple myeloma. Leuk Lymphoma, 2009; 50(5):809–15; doi.org/10.1080/10428190902802323.

Shebl M, Khalil SME, Al-Gohani FS. Preparation, spectral characterization and antimicrobial activity of binary and ternary Fe (III), Co (II), Ni (II), Cu (II), Zn (II), Ce (III) and UO2 (VI) complexes of a thiocarbohydrazone ligand. J Mol Struct, 2010; 980(1–3):78–87; doi.org/10.1016/j.molstruc.2010.06.040.

Singh DP, Grover V, Rathi P, Jainb K. Trivalent transition metal complexes derived from carbohydrazide and dimedone. Arab J Chem, 2013; 10(2):S1795–S1801; doi.org/10.1016/j.arabjc.2013.07.004.

Singh NK, Singh SB. Synthesis, characterization and biological properties of manganese (II), cobalt (II), nickel (II), copper (II), zinc (II), chromium (III) and iron (III) complexes with a new thiosemicarbazide derivative. Ind J Chem, 2001; 40(10):1070–75.

Subarkhan MM, Ramesh R. Binuclear ruthenium (III) bis (thiosemicarbazone) complexes: synthesis, spectral, electrochemical studies and catalytic oxidation of alcohol. Spectrochim Acta A Mol Biomol Spectrosc, 2015; 138:264–70; doi.org/10.1016/j.saa.2014.11.039.

Tang J, Yin HY, Zhang JL. Luminescent zinc complexes as bioprobes for imaging molecular events in live cells. In, In Organic and organometallic transition metal complexes with biological molecules and living cells, (pp 1–35), 2017; doi.org/10.1016/B978-0-12-803814-7.00001-0.

Veiga N, Alvarez N, CastellanoEE, Ellena J, Facchin G, Torre MH. Comparative study of antioxidant and pro-oxidant properties of homoleptic and heteroleptic copper complexes with amino acids, dipeptides and 1, 10-phenanthroline: the quest for antitumor compounds. Molecules, 2021; 26(1):6520; doi.org/10.3390/molecules26216520.

Vera-Ramirez L, Sanchez-Rovira P, Ramirez-Tortosa MC, Ramirez-Tortosa CL, Granados-Principal S, Lorente JA, Quiles JL. Free radicals in breast carcinogenesis, breast cancer progression and cancer stem cells. Biological bases to develop oxidative-based therapies. Crit Rev Oncol Hematol, 2011; 80(3):347–68; doi.org/10.1016/j.critrevonc.2011.01.004.

White MT, Dillingham MS. Iron–sulphur clusters in nucleic acid processing enzymes. Curr Opin Struct Biol, 2012; 22(1):94–100; doi.org/10.1016/j.sbi.2011.11.004.

Zhang C. Essential functions of iron-requiring proteins in DNA replication, repair and cell cycle control. Protein Cell, 2014; 5(10):750–60; doi 10.1007/s13238-014-00.

How to cite this article:
Aly SA, Eldourghamy A, El-Fiky BA, Megahed AA, El-Sayed WA, Abdalla EM, Elganzory HH. Synthesis, spectroscopic characterization, thermal studies, and molecular docking of novel Cr(III), Fe(III), and Co(II) complexes based on Schiff base: *In vitro* antibacterial and antitumor activities. J Appl Pharm Sci, 2023; 13(02):196–210.

SUPPLEMENTARY METERIALS

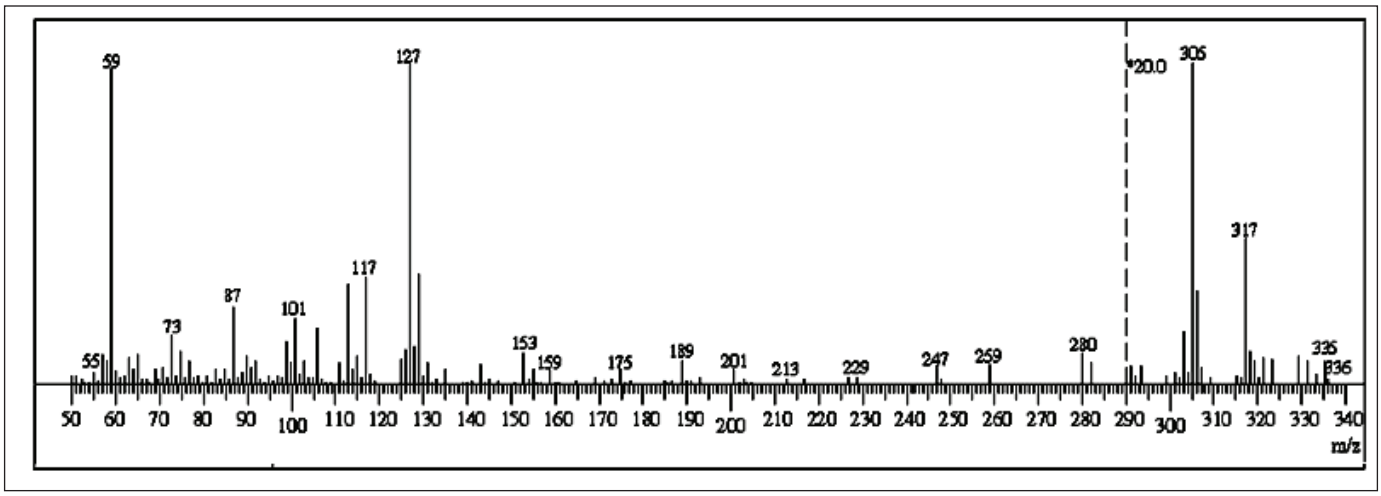

Figure S1. Mass spectrum of ligand.

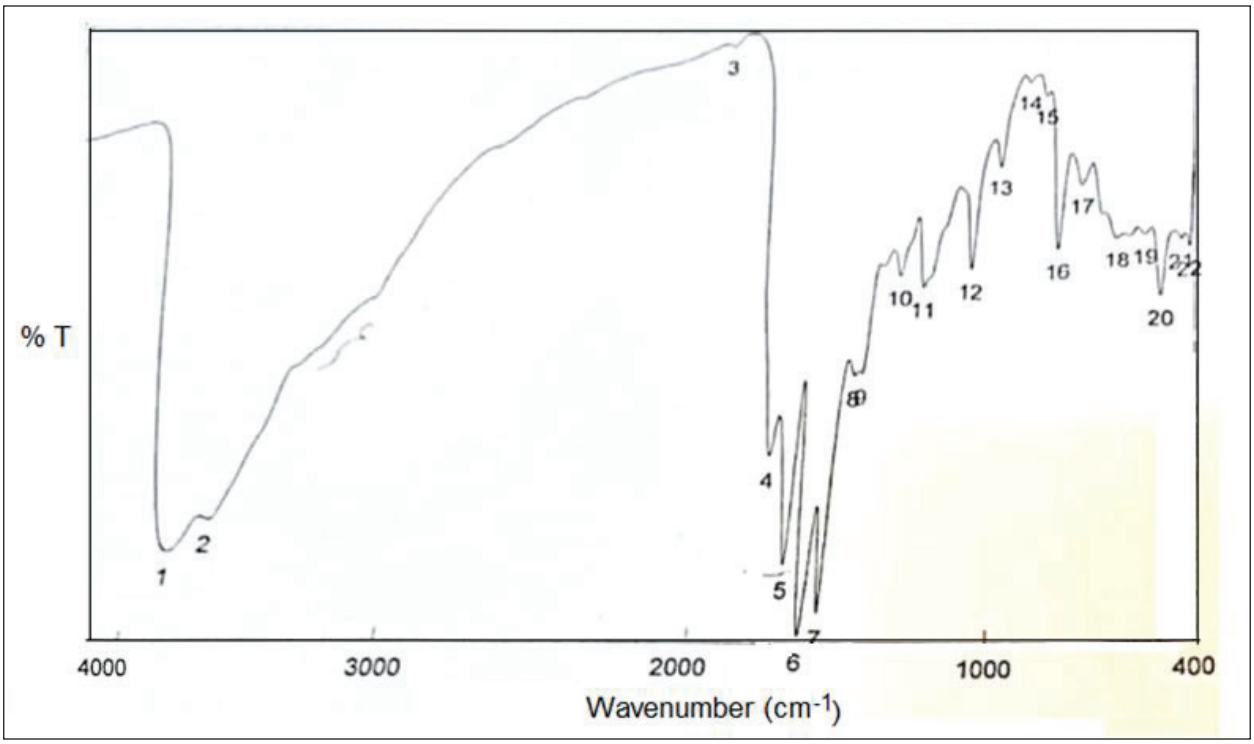

Figure S2. FT-IR spectra of Cr spectra of Cr(III) complexes.

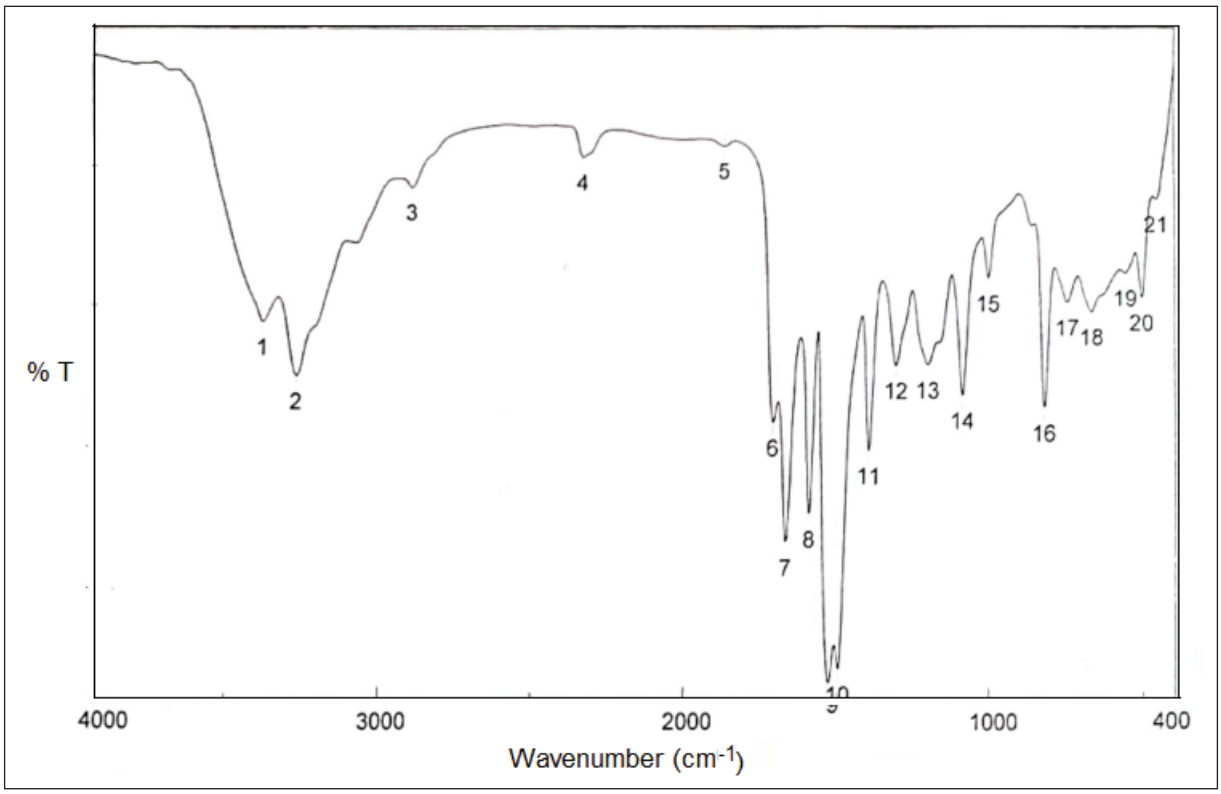

Figure S3. FT-IR spectra of Co(II) complexes.

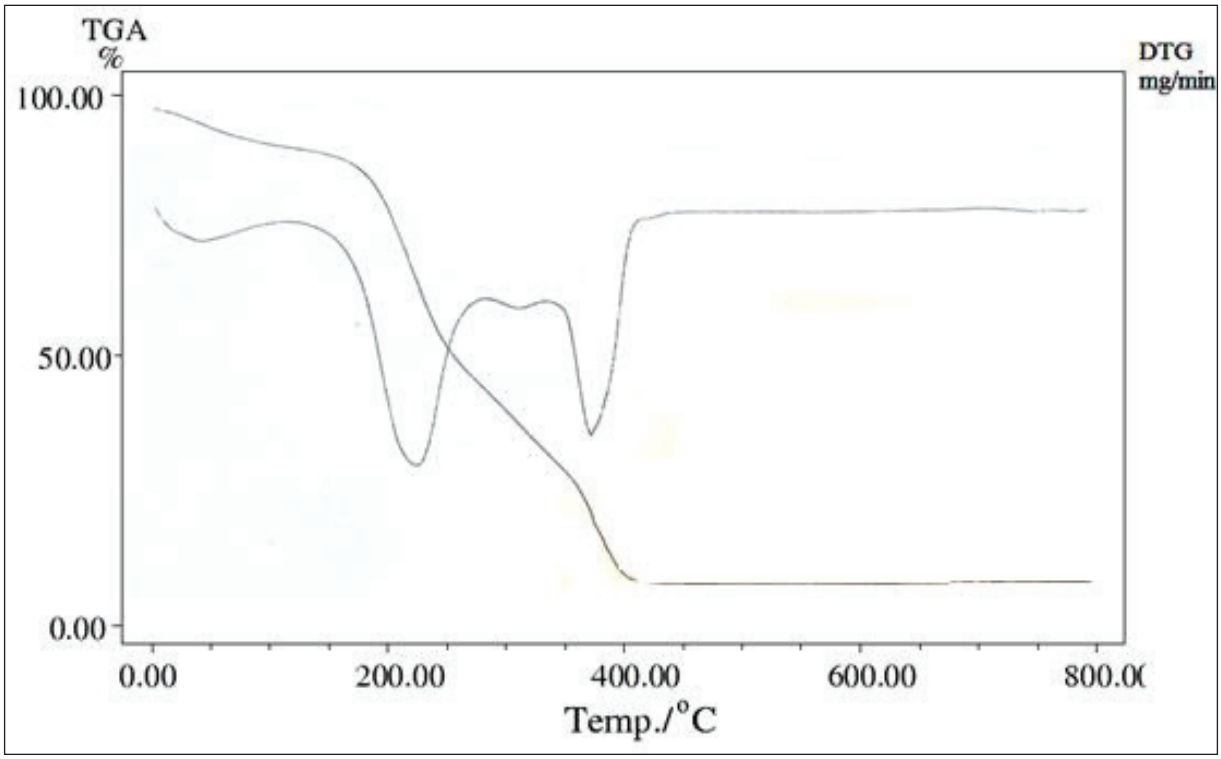

Figure S4. TGA/ DTG curves of the complex $[Cr(H_2L)_2Cl_2]ClEtOH$.